ELSEVIER

Composites Science and Technology 59 (1999) 2047–2054

COMPOSITES SCIENCE AND TECHNOLOGY

Experimental determination of the compressive strength of pultruded structural shapes

E.J. Barbero [a,*], S. Makkapati [b], J.S. Tomblin [c]

[a] *Mechanical and Aerospace Engineering, West Virginia University, Morgantown, WV 26506-6106, USA*
[b] *Ford Scientific Research Laboratories, Detroit, MI, USA*
[c] *Aerospace Engineering, Wichita State University, KS, USA*

Received 2 December 1998; received in revised form 7 March 1999; accepted 15 April 1999

Abstract

An existing coupon compression fixture was modified for testing cylindrical coupon samples of a pultruded material in compression. Then a new fixture was developed for testing full-sized structural shapes, which presents all the advantages of the coupon fixture. Particularly, splitting of the end of the sample is prevented while reducing the stress concentration factor at the ends, yielding compression failures at the center of the specimen. All the fiber reinforcements of structural shapes (CSM, ±45, and roving) were tested individually and combined to support the development of a simple model for compressive strength of structural shapes. A simple formula is developed for the prediction of the compressive strength of pultruded structural shapes. Comparisons between experimental data and predicted values are presented. © 1999 Elsevier Science Ltd. All rights reserved.

Keywords: E. Pultrusion; Structural shapes; Compressive strength; Testing; Design equation

1. Introduction

Composite structural shapes are produced by pultrusion, with the geometry and material properties of the cross-section being fixed by the manufacturer. A broad selection of such shapes is offered [1–3]. Composite structural shapes are used because of their high strength to weight ratio, resistance to environmental deterioration, and lack of interference with electromagnetic radiation. Buckling controls the failure of current off-the-shelf structural shapes when used as columns [4–9] and beams [10–13]. For example, the buckling strength of a WF152 × 6.35 is 56.4 MPa [7] while the compressive strength reported here is 306.9 MPa. However, as these sections are optimized to increase their buckling load, the material compressive strength will be reached, thus, providing motivation for this study. Interaction between buckling and compressive strength is likely to occur if both values are similar [6].

Fiber-reinforced structural shapes are formed by pultruding a stack of several fiber systems. Basically, roving (unidirectional fibers) are arranged in layers separated by continuous strand-mat (CSM) and stitched-mat layers. The layered structure exists only for the fibers because all the impregnated fibers are cured at once in the die. But the rovings are always separated by CSM or stitched-mat layers. Otherwise, internal cracking of the thick pultruded shapes would occur. Therefore, we studied the compressive strength of each fiber architecture separately and then combined all the results to estimate the strength of the whole laminate.

2. Coupon compression fixture

The testing of coupons of pultruded structural shapes in compression presents unique problems in addition to the general problem associated with the testing of composite materials in compression. In general, compression testing is difficult because the composite material has high longitudinal strength and low transverse strength. Therefore, direct end loading of samples (ASTM 695) is not possible because the ends of the specimen separate (splitting) and the property measured is the composite bearing strength rather than the actual compressive strength. This problem also occurs in the testing of full-size structural shapes. In structural applications this may not be a problem if the load is introduced gradually by a proper connection detail.

* Corresponding author.

0266-3538/99/$ - see front matter
PII: S0266-3538(99)00063-9

Many fixtures have been developed to prevent splitting at the ends of the specimen by introducing restrictions to the lateral expansion of the specimen at the ends [14–18]. In most fixtures this is accomplished by end-tabs, but the use of end-tabs is very time consuming. Since pultruded materials have high variability in material properties from point to point, a large sample population is needed to obtain good estimates of average, standard deviation, and so on. Therefore, it becomes important to reduce the cost and time of specimen preparation, without sacrificing accuracy.

Of all the test methods available, we selected a modification of ASTM D695 [19–20] because it eliminates splitting at the ends without the use of tabs. We also opted for cylindrical rod samples to simplify specimen preparation. Furthermore, shear tests are greatly simplified by using rod samples. The samples are cut and milled at the ends to have a flat surface perpendicular to the length of the sample. The original compression fixture was modified in this project for testing cylindrical samples (rods). In the case of rod samples, the ends are machined flat with a lathe. A milling machine is used for rectangular samples. No end tabs are used, and the sample is restrained laterally only at the perimeter of the surface in contact with the compression plates of the machine (Fig. 1). Then, the entire length of the sample is available for testing, and the center of the sample is farther from the ends, where any end effects may disturb the stress field. Therefore, compression failures at or near the center of the specimen are free of spurious end effects.

One of the modifications made to the original fixture is to rigidly attach the fixture to a universal testing system (UTS). The fixture was aligned using a rectangular aluminum sample with four strain gages, one on each side. By loading the aluminum sample and checking the strain-load plot of the four gages, the fixture was shimmed until perfectly aligned. Since structural shapes are relatively thick (9.5–12.7 mm), buckling of the sample is not a problem. Therefore, we removed the guide pins that were used in the original fixture. This allowed easier access to strain-gage the samples.

3. Pultruded rod samples

Pultruded rods (9.5-mm diameter) were produced at Cre^tive Pultrusions, Inc. The samples were labeled with a three-letter code (Table 1): the first letter indicates the volume fraction, the second the resin type, and the third the roving type. The three resins were: type (A) 2036-C polyester, type (B) D1419 vinyl ester, and type (C) 2036-C polyester with double amount of styrene, all produced by Ashland Chemicals. The three fibers were type (A) 102-AA-56 yield, type (B) 366-AD-133 yield, and type (C) 366-AC-250 yield, all E-glass produced by Owens Corning Fiberglass. Since the number of rovings must be an integer and the yield of various fiber types (56, 113, 250) are not multiples of each other, the fiber volume fractions, V_f, that can be achieved with different fiber types are not exactly the same. The resulting values are shown in Table 1. The compositions of the three resins are shown in Table 2. Since the solid content must be approximately constant during pultrusion, filler was added when the fiber volume fraction decreased, as indicated in Table 2.

Seventeen material combinations of pultruded rods were tested in compression with the coupon fixture modified for cylindrical samples. Seven replicates per material were tested, for a total of 119 samples. The sample length was 25 mm. The experimental results, including the 95% confidence interval, are shown in Table 3. The compressive strength of the matrix was measured using the same fixture and cylindrical matrix rods. The rods were produced by pouring resin into a 9.5-mm glass tube and curing it in an oven for 1 h at 150°C. The average experimental compressive strength for the matrix was $F_{\mathrm{mc}} = 44.785$ MPa.

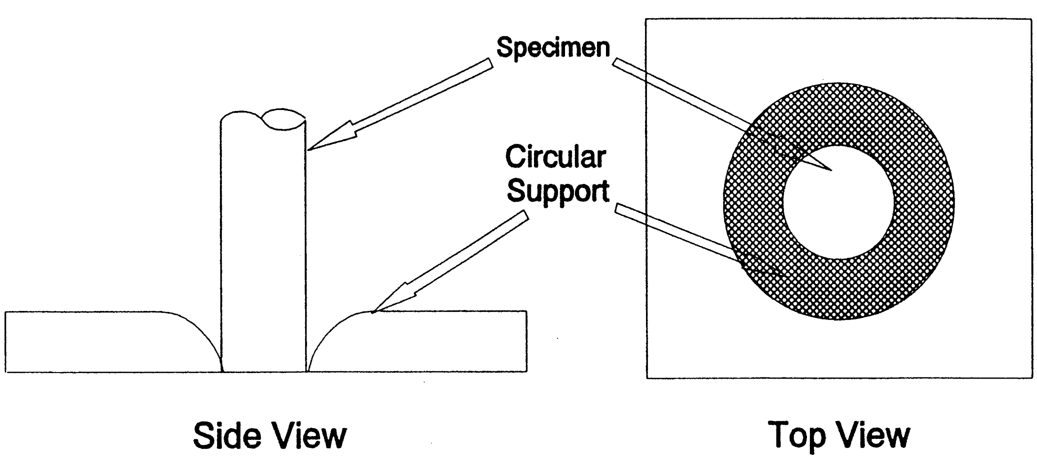

Fig. 1. Schematic of circular edge restraint for the new compression fixture.

Table 1
Materials used in pultruded rod samples. Resin codes are as follows: type (A) 2036C Polyester, type (B) D1419 vinyl ester, and type (C) 2036C-S polyester with double amount of styrene

Code	V_f	Resin	Fiber	No. roving	Fiber diameter (μm)
CAA	0.402	2036C	56	8	13
CAB	0.430	2036C	113	17	23
CAC	0.439	2036C	250	39	17
CBA	0.402	D1419	56	8	13
CBB	0.430	D1419	113	17	23
CBC	0.439	D1419	250	39	17
CCA	0.402	2036C-S	56	8	13
CCB	0.430	2036C-S	113	17	23
CCC	0.439	2036C-S	250	39	17
ACA	0.552	2036C-S	56	11	13
BCA	0.502	2036C-S	56	10	13
ACC	0.572	2036C-S	250	51	17
BCC	0.529	2036C-S	250	47	17
ABA	0.552	D1419	56	11	13
ABC	0.574	D1419	250	51	17
BBA	0.502	D1419	56	10	13
BBC	0.529	D1419	250	47	17

Table 2
Composition of polyester resin (code A, second letter in label) and vinyl ester resin (code B), with values of fiber volume fraction A, B and C (first letter in label) given in Table 1

Description	Amount	Polyester	Vinyl ester
Resin	90 kg	2036C	D1419
Release agent	0.9 kg	CP250	CP250
Added monomer	0.9 kg	Styrene	Styrene
Low temperature catalyst	544 g	P-16N	P-16N
High temperature catalyst	182 g	Trig 121	Trig 121
Kaolin clay filler	6.35 kg at V_f A	ASP-400	ASP-400
Kaolin clay filler	18.14 kg at V_f B	ASP-400	ASP-400
Kaolin clay filler	31.75 kg at V_f C	ASP-400	ASP-400

4. Coupon tests from structural shapes

Rectangular coupons were cut from flanges and webs of off-the-shelf structural shapes produced by Creative Pultrusions, Inc. using E-glass fibers and vinyl ester D1419 resin. The coupons were then tested in compression using the modified ASTM D-695 compressive fixture for rectangular samples [19–20]. Both modulus and compressive strength were recorded. A total of 126 samples were tested. The sample length was 25 mm. Seven replicates per test were used. Longitudinal and transverse samples from flange and web of four different wide-flange (WF) structural shapes (Table 4) were tested in compression. In addition, longitudinal and transverse samples from the flange of one box section were tested (see Table 4). The average stress is computed dividing the load by the area of the sample. The longitudinal values of average stress correlate well with the average stress values obtained from full-size testing of the same structural shapes (Table 5).

5. Full-size tests

When full-sized structural shapes were loaded directly with the flat plates of a universal testing system [21], the specimens split at the ends. Therefore, a special set of grips was developed during this investigation to avoid premature failure. Since the coupon fixture was successful for compression testing of pultruded materials, the full-size grips attempt to reproduce the features of the coupon fixture. However, mechanical constraint of the lateral expansion, like in the coupon fixture, cannot be directly implemented in a full-sized fixture because a very complex fixture would be required for each particular geometry of the cross-section. Furthermore, the thickness and shape of the cross-section are not completely uniform. Therefore, a rigid mechanical fixture would not exactly fit any structural shape.

The solution adopted was to fabricate a steel plate with a groove to fit each structural shape (Fig. 2). The groove is thicker than the walls of the structural shape to allow slightly different samples to fit. However, from the coupon fixture, it was found that positive restraint of the lateral expansion was needed in order to avoid splitting. The positive restraint was achieved by potting the structural shape into the groove with the aid of a room-temperature cure polyester resin, i.e. filling the space between the groove and the structural shape with the resin. The thin layer of polyester resin is confined between the walls of the groove in the steel plate and the structural shape. This provides sufficient restraint against splitting. The flexibility of the polyester resin helps reduce the stress concentration introduced by the confinement. With this fixture, failures occurred in compression rather than splitting and always near the center of the gage, as shown in Fig. 3. The specimen is potted with the polyester resin at both ends into the two grooved plates, then the specimen is aligned with the load cell and the swivel mechanism of the Universal Testing System (Baldwin 890 kN). The load and strains are recorded using a DAS-8 data acquisition system and LabTech Notebook [30] software on an MS-DOS PC.

Twelve tests of each type of shape were tested to failure, except for the WF152x9.52 mm for which only two samples could be tested because of limitations of the equipment. The total number of samples tested was 50. The sample length was 100 mm. The experimental results are shown in Table 5, where the 95% confidence interval is shown next to the failure load as a ±interval. The average stress was computed dividing the load by the area of the sample. Some of the stress values averaged over the whole cross-section (Table 5) are slightly

Table 3
Experimental values of misalignment angle, shear stiffness, strength and compressive strength, as well as predicted values of compressive strength for rod samples

Code	Standard deviation of misalignment Ω [deg]	G_{12} (MPa)	F_6 (MPa)	Compressive strength F_{1c} (MPa)		
				Experimental	Predicted	%Difference
CAA	3.4567	3462	40.57	477.74 ± 36.6	370.37	22
CAB	3.3875	3043	37.86	462.65 ± 16.6	343.26	26
CAC	3.3012	3383	38.53	489.74 ± 26.4	366.14	25
CBA	3.5308	4223	43.09	481.04 ± 25.7	406.28	16
CBB	3.3000	4224	43.09	521.56 ± 16.2	425.02	19
CBC	3.2795	4268	42.75	540.34 ± 20.0	426.02	21
CCA	3.3957	3487	43.33	523.74 ± 16.1	392.40	25
CCB	3.0542	3628	42.06	546.28 ± 10.7	418.25	23
CCC	3.1796	3487	39.86	494.88 ± 15.3	387.83	22
ACA	3.5954	4914	43.63	560.9 ± 35.1	425.59	24
BCA	3.3651	4703	42.10	537.05 ± 39.3	428.11	20
ACC	3.1120	5530	38.67	697.56 ± 26.7	449.55	36
BCC	3.6359	3220	38.21	623.21 ± 55.8	335.90	46
ABA	3.8051	3580	46.69	625.67 ± 46.5	385.78	38
ABC	3.4416	5160	41.33	579.04 ± 11.9	429.48	26
BBA	3.7010	5170	40.00	611.82 ± 37.5	400.36	35
BBC	3.3865	3300	40.68	578.8432.7	370.07	36

Table 4
Results for coupon samples cut from various structural shapes. In the label, the first number is the width of both flange and web; the second is the thickness of flange and web unless otherwise noted

Type	Direction	Panel	Experimental load (kN)	Average stress (MPa)
WF 101×6.35 mm	Longitudinal	Flange	54.4 ± 4.9	337
		Web	48.0 ± 2.5	298
	Transverse	Flange	17.5 ± 0.7	109
		Web	25.1 ± 0.9	156
WF 101×6.35 mm with ±45	Longitudinal	Flange	42.1 ± 2.6	261
		Web	36.1 ± 1.6	224
	Transverse	Flange	11.9 ± 0.2	74
		Web	18.9 ± 0.6	117
WF 152×6.35 mm (t_w = 7.15 mm)	Longitudinal	Flange	45.6 ± 6.2	283
		Web	46.8 ± 2.9	290
	Transverse	Flange	19.1 ± 1.4	118
		Web	27.9 ± 1.7	173
WF 152×9.52 mm	Longitudinal	Flange	46.3 ± 2.9	252
		Web	42.3 ± 0.9	225
	Transverse	Flange	21.0 ± 1.2	115
		Web	24.6 ± 0.9	130
Box 101×5.58 mm	Longitudinal		40.8 ± 6.6	287
	Transverse		10.4 ± 0.3	73

Table 5
Comparison of experimental full-size loads with the results of the simplified equations [Eqs. (8) and (9)]

Section	N_R	TEX (g/km)	F^*_{1c} (MPa)	Pred. (kN)	Exp. (kN)	% Difference	Average stress (MPa)
WF101×6.35	232	4392	1211	493.6	590.5	−16.41	306.90
WF101×6.35±45	232	4392	1211	493.6	412.8	19.57	244.15
WF152×6.35 (t_w = 7.15)	182	8861	1202	775.4	685.4	13.13	227.16
WF152×9.52	255	8861	1202	1086.4	1026.2	5.87	236.39
Box101×5.58	288	4392	1211	612.7	584.8	4.77	259.41

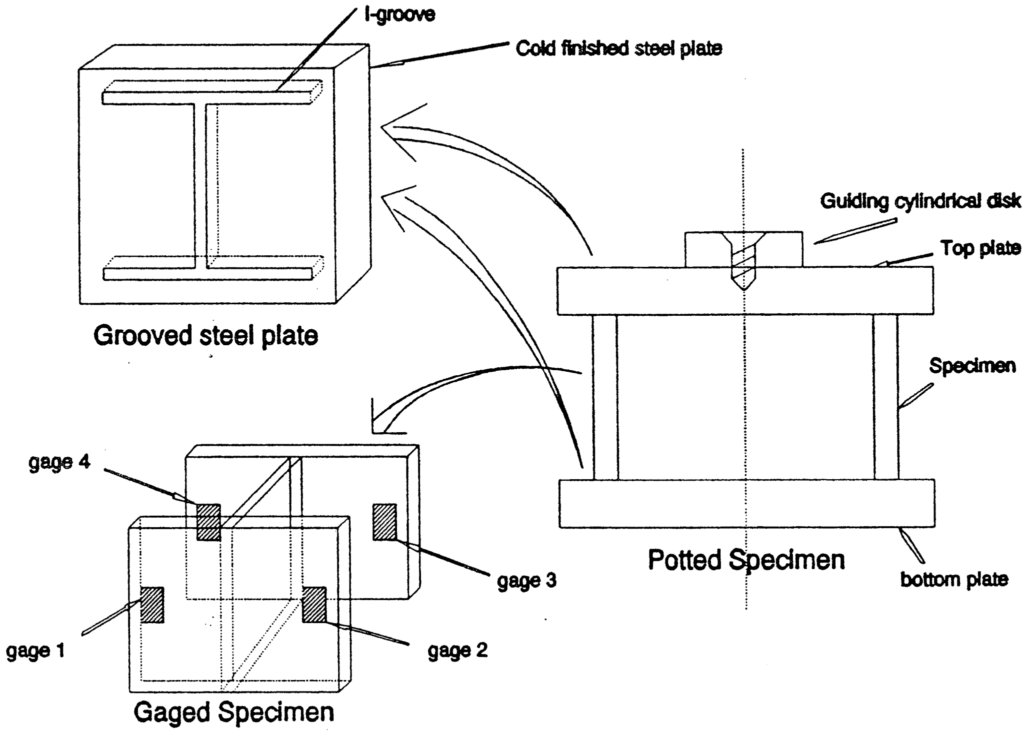

Fig. 2. Grooved steel plates used for full-sized testing and position of the strain gages on the sample.

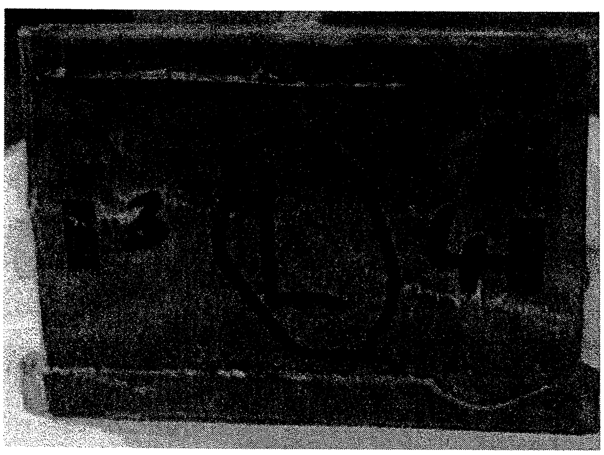

Fig. 3. Full-sized sample showing compressive failure close to the center of the specimen.

lower than the coupon values (Table 4). This results from the flange-web intersection being weaker than the panels (flange and web) because the reinforcement tends to migrate away from the corners during pultrusion.

6. Shear behavior of a unidirectional composite

The use of rod samples simplified the determination of shear properties for the unidirectional roving-reinforced material. Both the shear stiffness and strength were determined experimentally by using a torsion test [22] and cylindrical rod samples. In this investigation, the shear stress–strain curve is represented [23] by

$$\tau_{12} = F_6 \tan h\left(\frac{G_{12}}{F_6}\gamma_{12}\right) \quad (1)$$

where G_{12} is the shear stiffness and F_6 is the shear strength of the composite material. Both G_{12} and F_6 are computed from the measured torque-twist experimental data. Eq. (1) is integrated over the cross-section of the sample to obtain the torque-twist relationship. Then, the initial shear modulus G_{12} is obtained from linear regression of the linear portion of the curve. The shear strength F_6 is obtained by comparing the predicted and experimental asymptotic values of torque for large shear strains. The results for all material combinations are shown in Table 3.

7. Fiber misalignment and compressive strength in rod samples

The distribution of fiber misalignment of all rod samples was measured by an optical technique [24]. The data can be represented closely by a Gaussian distribution with zero mean value [25]. Then, the data are completely represented by the standard deviation Ω, with values reported in Table 3. The standard deviation of fiber misalignment is necessary to predict the compressive strength of the rod samples according to [26–27]

$$F_{1c} = G_{12}\left(\frac{\chi}{a}+1\right)^{b}$$
$$\chi = \frac{G_{12}\Omega}{F_6} \qquad (2)$$

with $a = 0.21$ and $b = -0.69$. A comparison between predicted and experimental results is presented in Table 3.

8. Compressive strength of $\pm\theta$ layers

Existing models for compressive strength of $\pm\theta$ layers [28] indicate that shear, rather than compression, dominates the failure of $\pm\theta$ layers when the angle is larger than 30°. Since most pultruded shapes use $\pm 45°$, the shear strength of the $\pm\theta$ layers is the actual limit of the load carrying capacity of those layers. Plates of ± 45-stitched mat were produced using a hot press (PHI model 150R). The same resin and CSM type used in commercial structural shapes were used for the samples (vinyl ester D-1419) and the stitched mat was of 4.425 kg/m^2 (4.5 oz/ft^2) weight. The resin was prepared as for the production of structural shapes (Table 2).

By varying the number of mat layers included in the plates (4.76 mm thick), it was possible to obtain samples with two values of fiber content, 22.82 vol% and 38.02 vol%. The samples were tested in compression with the coupon fixture for rectangular samples. For each value of fiber volume fraction, seven samples were tested. The experimental compressive strength $F_{xc\theta}$ and modulus $E_{x\theta}$ (including the 95% confidence interval) are shown in Table 6. Also, seven samples for each value of fiber volume fraction were tested to determine the shear strength $F_{xy\theta}$ of the ± 45 layers. The test method used was the off-axis test [26]. The experimental values (including the 95% confidence interval) are shown in Table 6. It must be noted that the strength of the ± 45 layers reported in Table 6 are much lower than the strength of the roving samples reported in Table 3. This indicates that the ± 45 layers fail well before than the roving layers during loading of structural shapes.

9. CSM compressive strength

Plates of CSM material were produced using a hot press (PHI model 150R). The same resin and CSM type used in commercial structural shape were used for the samples (vinyl ester D-1419 resin and 17 g/m^2 CSM (1/2 oz/yd^2).) The resin was prepared as for the production of structural shapes (Table 2). By varying the number of CSM layers included in the plates (4.76 mm thick), it was possible to obtain samples with two values of fiber volume fraction, 16.5 and 25%. The samples were tested in compression using the coupon fixture for rectangular samples. Although CSM is supposed to be random, the fibers have a slight preferential orientation along the length of the CSM roll. For each value of fiber volume fraction, four samples were cut in the direction of the length of the CSM roll and four samples transverse to it. Experimental values of compressive strength FCSM and modulus ECSM are shown in Table 7.

Since pultruded columns have the CSM oriented with the roll direction along the length of the column, the highest experimental value should be used. Note that the strength values reported for CSM are much lower than the strength of the roving reported in Table 3. This indicates that the CSM fails well before the roving during loading of structural shapes.

10. A simple model

The experimental data shown indicate that the compressive strength of CSM and $\pm\theta$ layers (Tables 6 and 7) are much lower than the compressive strength of the roving (Table 3). This was confirmed by performing a progressive failure analysis of each full-size sample following a procedure similar to that described by Kim et al. [29]. Taking into account that the roving carry the load up to failure, after all the CSM and $\pm\theta$ layers have failed, it is possible to derive a simple formula for the compressive strength of structural shapes. The following assumptions are made:

1. the roving layers carry the entire load, after all the CSM and $\pm\theta$ layers have failed;
2. Poisson's effects are negligible;
3. The compressive strength of the roving layers is proportional to the fiber volume fraction;
4. The fiber volume fraction is the same for all the roving layers in the cross-section.

Based on these assumptions, the stress–strain law for compression of a roving layer is

Table 6
Compressive and shear strength of ± 45 layers

V_f	$E_{x\theta}$ (GPa)	$F_{XC}\theta$ (MPa)	$F_{XY}\theta$ (MPa)
22.82	1.140	101.8 ± 4.6	48.125
38.02	1.674	100.3 ± 2.5	45.570

Table 7
Strength and stiffness of CSM layers

V_f	Direction	F_{CSM} (MPa)	E_{CSM} (GPa)
16.5	Longitudinal	137.8 ± 3.1	8.58 ± 0.17
25.0	Longitudinal	179.2 ± 14.2	10.82 ± 0.21
16.5	Transverse	128.2 ± 3.4	7.04 ± 0.77
25.0	Transverse	160.8 ± 5.9	9.94 ± 0.46

$$\sigma_x = E_1 \varepsilon_x \tag{3}$$

where E_1 is the stiffness in the fiber direction of the roving layers. The failure of the cross-section occurs when the stress in the roving layers reaches the value of the compressive strength F_{1c}. The total load carried by the section at failure is

$$P = F_{1c} \sum_{i=1}^{n} b_i t_i \tag{4}$$

where n is the number of panels (web and flanges) of the cross-section, b_i are the width and thickness of the ith panel, respectively. The latter can be computed as [26]

$$t_i = \frac{N_i}{b_i} \frac{\mathrm{TEX}}{\rho^V f} \tag{5}$$

where N_i is the number of roving in the panel, TEX is the weight per unit length of the roving used, ρ is the density of the fibers, and V_f is the fiber volume fraction. Substituting into the expression for P, the compressive load of the structural shape is

$$P = \frac{F_{1c}}{V_f} \frac{\mathrm{TEX}}{\rho} \sum_{i=1}^{n} N_i \tag{6}$$

The summation of N_i is equal to the total number of roving in the cross-section N_R, which can be easily counted from the production schematic available from the manufacturer. Defining the specific roving compressive strength F_{1c}^* as the roving compressive strength (Table 8) divided by the fiber volume fraction

$$F_{1c}^* = \frac{F_{1c}}{V_f} \tag{7}$$

we can write an expression for the compressive strength of the structural shape as

$$P = \frac{F_{1c}^* N_R \mathrm{TEX}}{1000\rho} \tag{8}$$

with F_{1c}^* in MPa, TEX in g/km, and ρ in g/cc (2.5 g/cc for E-glass) and P in Newton. In US customary units

$$P = \frac{F_{1c}^* N_R}{36 Y \rho} \tag{9}$$

where Y is the yield in yd/lb., $\rho = 0.09032$ lb./in^3 and P in lb. TEX and yield are related as $\mathrm{TEX} = 496,238/Y$ (see [26], p.64). The specific roving compressive strength F_{1c}^* is a material property for each type of roving, with values tabulated for the most common types of pultruded materials (Table 8). The values in Table 8 have been determined experimentally using rod samples reported in Table 3. In Table 8, vinyl ester is Ashland D-1419, polyester is Ashland 2036-C, and brittle polyester is Ashland 2036-C with twice the normal amount of styrene (Table 2).

Using the simplified equations [Eqs. (8) and (9)] the compressive strength of the structural shapes were computed and compared to the experimental values in Table 5. While some differences exist between the predicted and experimental values, Eqs. (8) and (9) follow the trend quite well and predict the experimental load with considerable accuracy. It must be noted that strength values in general, and compressive values in particular, are quite difficult to predict and measure. Therefore, the differences observed are considered small compared to other work in the literature. For example, Rosen's equation [31] would over predict the compressive strength by about 300% for the materials used in this study.

The average strength of the cross-section can be computed as the load [Eq. (8)] divided by the area of the cross-section

$$F_{xc} = \frac{F_{1c}^* N_R \mathrm{TEX}}{1000\rho \Sigma b_i t_i} \tag{10}$$

While the average strength can be used for design, it must be noted that this is an apparent value. No point of the cross-section experiences that amount of stress. Rather, the roving experience stress equal to F_{1c} at failure.

Table 8
Specific roving compressive strength for most common pultruded materials

Resin type	Roving type	Fiber volume fraction	F_{1c}^* (MPa)	F_{1c}^* (ksi)
Vinyl ester	56	40.2	1202	174
Vinyl ester	113	43.0	1211	176
Vinyl ester	250	43.9	1227	178
Polyester	56	40.2	1188	172
Polyester	113	43.0	1074	156
Polyester	250	43.9	1111	161
Brittle polyester	56	40.2	1308	190
Brittle polyester	113	43.0	1270	184
Brittle polyester	250	43.9	1125	163

11. Conclusions

The compressive strength of full-size structural shapes was successfully measured using a new fixture developed in this project. The compressive values obtained from full size samples correlate well with values obtained from coupons cut from the same samples and tested with an existing fixture for coupons. The coupon fixture was successfully modified for rod samples required in this investigation. Compressive strength was shown to be dominated by the roving. A simple formula was derived to predict the compressive strength of full-size structural shapes simply by counting the number of roving in the cross-section. The formula relies on experimental data from pultruded unidirectional rod samples of the same resin and roving as used in the structural shape. Alternatively, compressive strength of the roving can be predicted using measured values of standard deviation of fiber misalignment, and shear stiffness and strength. Correlation between predicted and experimental values was good.

Acknowledgements

The financial support of the West Virginia Division of Highways and the Federal Highways Administration through contract FPN FRP-9420 and SPN T-699-FRP-1 is appreciated. Thanks to J. Justice (FHWA), J. Brunel and J. Walker (WVDOH), for valuable suggestions during monitoring of the project. Thanks to M. Al-Megdad and R. Allison of Creative Pultrusions, Inc., J. Gauchell of Owens Corning and J. Mitrey of Ashland Chemical for their help in the production of the samples. Thanks to P. Dutta of CRREL, NH for help testing the largest samples and to E. Dede and J. Anderson for helping during production and testing of coupon samples.

References

[1] PULTEX Design Guide, Creative Pultrusions, Alum Bank, PA, 1989.
[2] Strongwell design manual. Bristol (VA): Strongwell, 1994.
[3] Bedford RP design guide. Bedford (PA): Bedford Reinforced Plastics, Inc., 1993.
[4] Banks WM, Rhodes J. The instability of composite sections. In: 2nd Int. Conf. on Composite Structures, Paisley, UK: Elsevier 1983. p. 442–52.
[5] Barbero EJ, Tomblin J. A phenomenological design equation for FRP columns with interaction between local and global buckling. Thin-Walled Structures 1994;18:117–31.
[6] Barbero EJ, Dede E, Jones S. Experimental verification of buckling-mode interaction in intermediate-length composite columns. Int J Solid Struct, in press.
[7] Barbero EJ, DeVivo L. Beam-column design equations for wide-flange pultruded structural shapes. ASCE J Composites in Construction, in press.
[8] Pecce M, Lazzaro F, Cosenza E. Local buckling of FRP profiles: experimental results and numerical analyses, European conference on composite materials ECCM-8, 331–338, Napoli, Italy, 1998.
[9] Yuan RL, Hashen Z, Green A, Bisarnsin T. Fiber-reinforced plastic composite columns. In: Iyer SL, editor. Adv. Composite Materials in Civil Eng. Structures. Las Vegas, NV: ASCE, 1991. p. 205–11.
[10] Bank LC, Nadipelli M, Gentry TR. Local buckling and failure of pultruded fiber-reinforced plastic beams, 1993 ASME Winter Annual Meeting, New Orleans, LA, 28 November–3 December, MD-Vol. 46, NY: ASME, 1993. p. 499–519.
[11] Barbero EJ, Fu S-H, Raftoyiannis I. Ultimate bending strength of composite beams. ASCE J of Materials in Civil Engineering 1991;3(4):292–306.
[12] Kabir MZ, Sherbourne AN. Lateral-torsional buckling of post-local buckled fibrous composite beams. ASCE J Eng Mechanics 1998;124(7):754–64.
[13] Davalos JF, Qiao P. Engineering design analysis equations for local buckling of FRP structural shapes. 2nd Int. Conf. on Composites in Infrastructure, 2, 248–260, Tucson, AZ, 1998.
[14] Häberle JG. Strength and failure mechanisms of unidirectional carbon fibre-reinforced plastics under axial compression. Thesis, Imperial College, London, UK, 1991.
[15] Welsh JS, Adams DF. Unidirectional composite compression strengths obtained by testing mini-sandwich, angle-, and cross-ply laminates. FAA report UW-CMRG-R-95-106, Federal Aviation Administration, NJ, 1995.
[16] Welsh JS, Adams DF. Current status of compression test methods for composite materials. Sampe J 1998;33(1):35–43.
[17] Tomblin JS, Hooper E, Bowman K, Ng Y, Smyth T, Showers D. Material qualification methodology for epoxy-based prepreg composite material systems. AGATE report, NIAR, Wichita, KS, 1998.
[18] Grooves SE, Highsmith AL. Compression response of composite structures, ASTM STP 1185, ASTM, Philadelphia, PA, 1994.
[19] Gurdal Z, Starbuck JM. Compressive characterization of unidirectional composite material. In: Sih GC, editor. Analytical and testing methodologies for design with advanced materials. Elsevier, 1988. p. 337–47.
[20] Starbuck JM, Gurdal Z. A procedure for accurate determination of elastic properties for unidirectional composite materials. In: Proceedings of the American Society for Composites, 3rd Technical conference on "Integrated Composites Technology", 25–29 September 1988.
[21] Tomblin JS. A universal design equation for pultruded composite columns. Thesis, West Virginia University, 1991.
[22] Sonti S, Barbero EJ, Winegardner T. Determination of shear properties for RP pultruded composites. J Reinforced Plastics and Composites 1995;14:390–401.
[23] Barbero EJ, Tomblin JS. A damage mechanics model for compression strength of composites. Int J Solid Structures 1996; 33(29):4379–93.
[24] Yurgartis SW. Measurement of small angle fiber misalignments in continuous fiber composites. Composites Science and Technology 1987;30:279–93.
[25] Tomblin JS, Barbero EJ. Statistical microbuckling propagation model for compressive strength prediction of fiber reinforced composites, ASTM STP 1242, 1997. p. 151–67.
[26] Barbero EJ. Introduction to composite materials design. Philadelphia: Taylor and Francis, 1998.
[27] Barbero EJ. Prediction of compression strength of unidirectional polymer matrix composites. J Composite Materials 1998; 32(5):483–502.
[28] Shuart MJ. Short-wavelength buckling and shear failures for compression loaded composite laminates. NASA TM - 87640, NASA Langley Research Center, Hampton, VA, 1985.
[29] Kim Y, Davalos JF, Barbero EJ. Progressive failure analysis of laminated composite beams. J Composite Materials 1996; 30(5):536–60.
[30] Labtech Notebook, Laboratory Technologies co., Wilmington, MA, 1994.
[31] Rosen BW. Fiber composite materials. Metals Park, OH: American Society for Metals, 1965 [Chapter 3].